Arabian Journal of Geosciences (2020) 13: 507
https://doi.org/10.1007/s12517-020-05515-3

ORIGINAL PAPER

Source rock properties and pore structural framework of the gas-prone Lower Permian shales in the Jharia basin, India

Bodhisatwa Hazra[1] · David A. Wood[2] · Pradeep K. Singh[1] · Ashok K. Singh[1] · Om Prakash Kumar[1] · Gaurav Raghuvanshi[1] · Deependra Pratap Singh[1] · Prasenjeet Chakraborty[1] · Pudi Srinivasa Rao[3] · Koushik Mahanta[3] · Gajanan Sahu[1]

Received: 20 February 2020 / Accepted: 3 June 2020 / Published online: 19 June 2020

Abstract
This paper examines the source rock potential and pore structural framework of Lower Permian shales belonging to Barren Measures and Barakar Formations of Jharia basin, eastern India. The Jharia basin contains prolific coking-coal reserves and, consequently, the organic-matter in this basin tends to be mature. Open system pyrolysis analysis reveals that the Barakar Formation shales are thermally more mature and organic-rich than the Barren Measures Formation. Analysis reveals that shales of the Barren Measures possess "fair" to "good" oil generation potential. The more mature shales of the Barakar Formation are gas prone. Detailed pore scale distribution and fractal metrics determined by low-pressure N_2 gas adsorption are observed to be higher for the Barren Measures Formation than the more mature and organically rich Barakar Formation shales possibly due to the inability of N_2 gas to access the ultrafine components of the complex pores in the Barakar Formation shales. Substantial concentration of pores, organic-rich character, and thermal maturity levels indicates that the studied horizons have unconventional source rock properties.

Keywords Porous structures · Fractal dimensions · Source rock · Rock-Eval · N_2 gas adsorption

Introduction

Organic-rich shales, in recent years, have emerged as a source of excitement for researchers dealing with petroleum-systems, as these represent self-contained petroleum systems with vast oil and gas resources (Schmoker 1995; Loucks et al. 2009, 2012; Jarvie 2012a, b; Peters et al. 2016; Wood and Hazra 2017a). Beyond acting as sources of unconventional oil and gas, shale and other organic-rich reservoirs have also emerged as attractive targets for carbon dioxide (CO_2) sequestration for combating the rising CO_2 levels in the atmosphere (Vishal et al. 2013a, b, 2019; Godec et al. 2013; Merey and Sinayuc 2016). The factors which directly control the potential of shale to act as petroleum systems or CO_2 sequestrating horizons are its organic-matter richness, kerogen type, thermal maturity of organic-matter, and the nature of pore structures within them which holds the gas/oil and can be possible sites for CO_2 storage (Tissot and Welte 1978; Jarvie et al. 2007; Mastalerz et al. 2013; Hazra et al. 2019a).

For predicting the source rock properties, the Rock-Eval technique is used extensively by researchers, as it allows fast and reproducible analysis of samples, producing set-of vital source rock parameters utilizing only small sample-amounts for the experiments (Carvajal-Ortiz and Gentzis 2015). The pore structures within shales on the other hand control the mechanism of gas adsorption-desorption and mode of fluid-flow (Loucks et al. 2009). Thorough evaluation and depiction of shale-porosity are thus crucial for assessing the oil and gas present within them and to understand their storage capacity (Zhang et al. 2012; Wood and Hazra 2017b; Hazra et al. 2019b). While different techniques exist to map pore structures in shales, in recent years, subcritical gas-adsorption techniques, using nitrogen (N_2), have emerged as convenient tools for distinguishing a range of pore-size components within the pore-scale distribution of shales (Ross and Bustin 2009; Yang

Responsible Editor: Santanu Banerjee

✉ Bodhisatwa Hazra
bodhisatwa.hazra@gmail.com

1 Coal Petrology Section, RQA Research Group, CSIR-Central Institute of Mining and Fuel Research, Dhanbad, India

2 DWA Energy, Bassingham, Lincolnshire, UK

3 Natural Resource Division, Tata Steel Limited, Jamshedpur, India

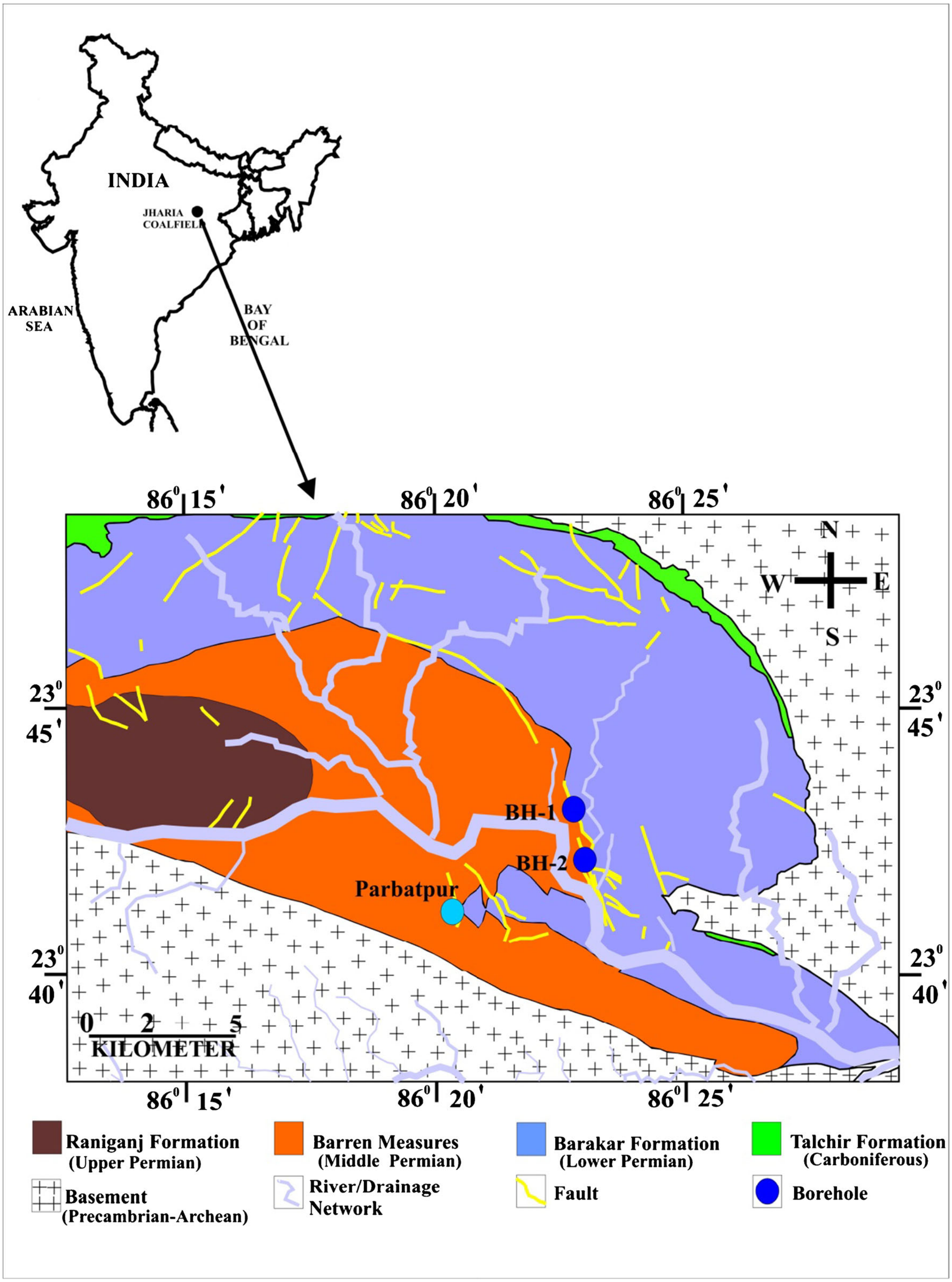

Fig. 1 Geographical position, geological features, formations, and sampling locations in Jharia basin (modified after Fox 1930; CIL 1993)

et al. 2014, 2016a, b; Holmes et al. 2017; Psarras et al. 2017; Hazra et al. 2018a).

Fractal dimensions calculated from information derived from low-pressure N_2 adsorption are successfully assessed to characterize the complex pore structures in organic-sedimentary rocks (Yao et al. 2008; Wood and Hazra 2017b). Recent works have also revealed the existence of two well-defined fractal indices in shales, corresponding to

Table 1 Jharia basin shale samples from wells A1 and A2: details and depths

Formation	Borehole	Sample ID	Depth (meters)
Barren Measures Formation	A1	BM-Sh-1	31.50–31.65 m
		BM-Sh-2	44.50–44.65 m
		BM-Sh-3	65.55–65.70 m
		BM-Sh-4	86.50–86.65 m
		BM-Sh-5	92.65–92.80 m
		BM-Sh-6	106.55–106.70 m
		BM-Sh-7	115.31–115.46 m
		BM-Sh-8	123.78–123.93 m
		BM-Sh-9	131.65–131.80 m
		BM-Sh-10	146.56–146.71 m
		BM-Sh-11	167.65–167.80 m
		BM-Sh-12	173.65–173.80 m
Barakar Formation	A2	Br-Sh-13	634.50–634.60 m
		Br-Sh-14	636.10–636.25 m
		Br-Sh-15	652.61–652.80 m
		Br-Sh-16	661.10–661.30 m
		Br-Sh-17	686.40–686.60 m
		Br-Sh-18	688.66–688.86 m
		Br-Sh-19	710.20–710.40 m
		Br-Sh-20	710.40–710.64 m
		Br-Sh-21	754.25–754.45 m
		Br-Sh-22	755.20–755.40 m
		Br-Sh-23	756.47–756.67 m

the adsorption behaviors at lower-relative pressure (D1; P/P0 < 0.50) and higher relative pressure (D2; P/P0 > 0.50) intervals (Wang et al. 2016; Hazra et al. 2018a, b).

The inability of N_2 to penetrate at lower pressures and experimental temperatures conditions (− 196 °C) typically results in the undercounting of the ultrafine microporous components in organic-matter (Ross and Bustin 2009). This also leads to under-representation of the fractal-metric corresponding to the lower pressure zone. In this work, we examine the validity of fractal dimensions and pore structural data for several shale samples at different stages of thermal maturity and organic-matter contents using N_2 as adsorbate.

Currently, India is strongly dependent upon oil and gas imports to supply its growing domestic energy consumption and large population. In this regard, shale petroleum systems and coal bed methane (CBM) offer indigenous resources that could potentially be exploited (Vaid 2017) to help and support the country's energy needs. The United States Energy Information Administration (EIA 2013) calculated a total of approximately 584 trillion cubic feet risked shale gas-in-place in India. Among Damodar Valley basins, the Central Mine Planning and Design Institute of India estimated 45 trillion cubic feet of shale gas in 6 sub-basins of Jharia¸ Bokaro, North and South Karanpura, Raniganj, and Sohagpur (Press Information Bureau 2015). Consequently, source rock properties, organo-petrographic composition, mineralogical composition, methane storage capacity, and pore structural attributes of India's Permian shale beds are the focus of attention in several recent studies (Varma et al. 2014, 2015; Hazra et al. 2015, 2018a, b; Boruah and Ganapathi 2015; Mendhe et al. 2017). However, only a few studies have focused on source rock properties and pore structural frameworks of the Jharia basin shales.

In this work, we examine source rock properties and the pore structural framework of the Jharia basin shales. The Jharia basin is the most important of the Damodar Valley sub-basins in terms of its exploitable coking coals resources (Mishra and Cook 1992). This is because the coals in Jharia basin are thermally more mature than the coals from adjoining basins (Mishra et al. 1990). The Jharia basin is also known to be strategically important for having significant CBM resources. Peters (2000) prioritized the Jharia basin as a key Indian basin for potential CBM exploration. The organic-matter in the coals from Jharia basin has the desired thermal maturity to generate gaseous hydrocarbons. Therefore, studying the organic-matter within the shales of basin of the same geological age (Lower Permian) can also be beneficial for understanding their gaseous hydrocarbon generation and gas storage potential.

Regional geology

The Jharia basin, located in Jharkhand state of India, is one of several hydrocarbon (petroleum and coal) resource-bearing, sub-basins of Damodar Valley, eastern India because of its coking coal reserves (Fox 1930). Showing a sickle-shape like structure, it covers approximately an area of 450 km^2 (Peters 2000). The Jharia basin represents a half-graben structure (Chatterjee and Ghosh 1970), with an east-west trending basin axis that plunges westward. Furthermore, the southern-flank of the basin is abruptly curtailed by a major regional fault(southern-boundary-fault) with a throw of over 1500 m (GSI 1977).Exposures of all Lower Gondwana Formations of Permian age are present in the basin. The Upper Permian Raniganj Formation is also exposed in this basin (Peters 2000). The Barakar Formation contains the basin's most prolific coal resources with eighteen coal well-developed seams (Fox 1930). The Upper Permian Raniganj Formation also includes thirteen coal seams. The Barren Measures Formation, amid the Raniganj and Barakar Formations, is devoid of any coal and attains a maximum thickness of ~ 750 m (Mukhopadhyay et al. 2010). Igneous intrusions in the form of mica-peridotite and dolerite dykes and sills are quite common at various locations scattered across the basin. These intrusions have increased the rank of coals adjacent to them

Table 2 Source rock properties of Jharia Basin shales derived from Rock-Eval analysis

Sample Number	S1 (mg HC/g rock)	S2 (mg HC/g rock)	S3 (mg CO_2/g rock)	T_{max} (°C)	HI (mg HC/g TOC)	OI (mg CO_2/g TOC)	PC (wt%)	RC (wt%)	TOC (wt%)	RC/PC
BM-Sh-1	0.36	4.26	0.21	449	118	6	0.42	3.18	3.60	7.57
BM-Sh-2	0.13	2.61	1.35	442	88	45	0.33	2.64	2.97	8.00
BM-Sh-3	0.39	3.48	0.42	442	98	12	0.39	3.16	3.55	8.10
BM-Sh-4	0.56	5.86	0.22	447	117	4	0.59	4.43	5.02	7.51
BM-Sh-5	0.5	4.06	0.65	445	102	16	0.48	3.52	4.00	7.33
BM-Sh-6	0.45	5.93	0.66	446	143	16	0.62	3.52	4.14	5.68
BM-Sh-7	0.89	12.66	0.63	445	206	10	1.19	4.96	6.15	4.17
BM-Sh-8	0.36	5.83	0.36	449	118	7	0.57	4.37	4.94	7.67
BM-Sh-9	0.35	4.59	0.24	448	117	6	0.45	3.47	3.92	7.71
BM-Sh-10	0.11	1.78	0.3	457	73	12	0.18	2.27	2.45	12.61
BM-Sh-11	0.12	1.37	0.11	460	66	5	0.13	1.95	2.08	15.00
BM-Sh-12	0.78	8.7	0.53	449	171	10	0.9	4.19	5.09	4.66
Br-Sh-13	1.23	18.66	0.31	461	141	2	2.13	11.06	13.19	5.19
Br-Sh-14	0.49	10.11	38.53	469	79	301	2.05	10.75	12.80	5.24
Br-Sh-15	0.24	4.04	1.88	602	19	9	0.43	20.7	21.13	48.14
Br-Sh-16	0.56	5.56	4.94	569	32	29	0.67	16.65	17.32	24.85
Br-Sh-17	0.56	15.11	1.09	469	92	7	1.38	15.13	16.51	10.96
Br-Sh-18	0.56	13.11	1.57	473	75	9	1.27	16.13	17.40	12.70
Br-Sh-19	0.77	18.2	1.15	470	83	5	1.7	20.29	21.99	11.94
Br-Sh-20	1.19	16.39	0.57	470	91	3	1.53	16.54	18.07	10.81
Br-Sh-21	0.91	11.83	0.61	471	78	4	1.14	14.03	15.17	12.31
Br-Sh-22	0.69	6.62	0.85	477	59	8	0.69	10.51	11.20	15.23
Br-Sh-23	0.63	17.88	0.58	475	78	3	1.59	21.19	22.78	13.33

due to thermal metamorphism (Pareek 1965; Chakrabarti 1969; Singh et al. 2007, 2008, 2013).

The studied area is placed to the east of the Parbatpur area in the Jharia basin (Fig. 1). CBM potential was initially evaluated in the Parbatpur area 2 decades ago (Peters 2000). Since then, commercial activities focusing on CBM flow have centered on the Parbatpur and adjoining areas. Peters (2000) estimated the Parbatpur block to have approximately 24 billion cubic meters of CBM resources.

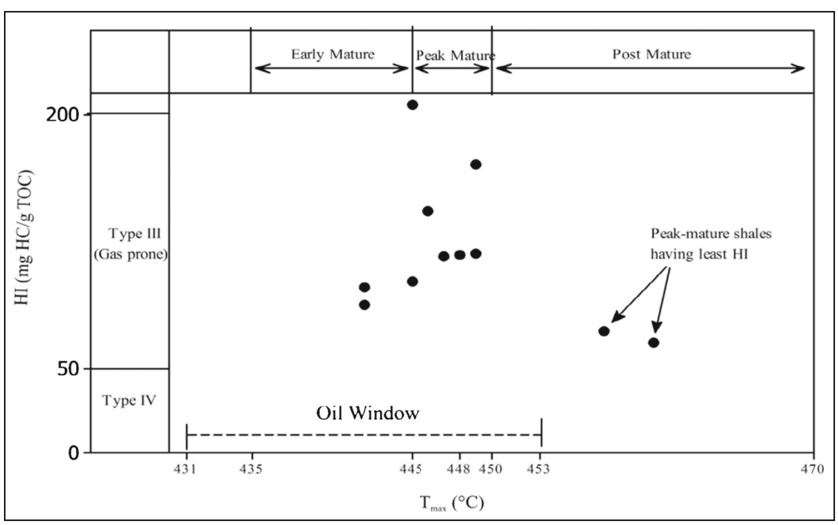

Fig. 2 HI vs T_{max} plot for the Barren Measures Formation Jharia Basin shale samples

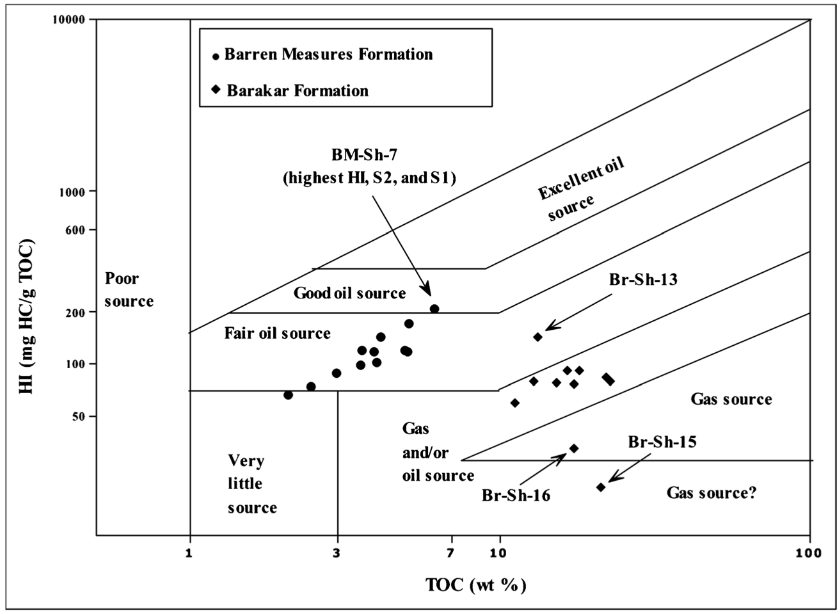

Fig. 3 HI vs TOC cross-plot for all Jharia Basin shale samples analyzed. The source rock-category compartments and boundaries displayed are modified after Jackson et al. 1985

Materials and methods

Sample details

Twenty-three shales, from different depths, were collected from two boreholes, A1 and A2 drilled in the Jharia basin, the locations of which are marked in Fig. 1. The depths and formations of these twenty-three samples are mentioned in Table 1.

Non-isothermal programmed-pyrolysis experiments

A Rock-Eval 6 equipment with built-in "basic method" was utilized for conducting pyrolysis and oxidation experiments on these Jharia Basin samples. These tests were performed to understand their petroleum-generation potential, organic richness, and thermal maturity. The details of the equipment and the method used are given in Lafargue et al. (1998) and Behar et al. (2001). Furthermore, since Jharia Basin shales predominantly comprises of type III-IV kerogen, revised analytical protocols as suggested by Hazra et al. (2017, 2019c, 2019d) were adopted.

Nitrogen (N_2) gas adsorption

Using N_2 gas at low pressures and temperatures, adsorption-desorption tests were performed with a Micromeritics-TriStar 3000 device. Sample sizes used were approximately 212 μm or less. Adsorption-desorption isotherms are based on a relative pressures (P/P0) range between 0.01 and 0.995. Sample

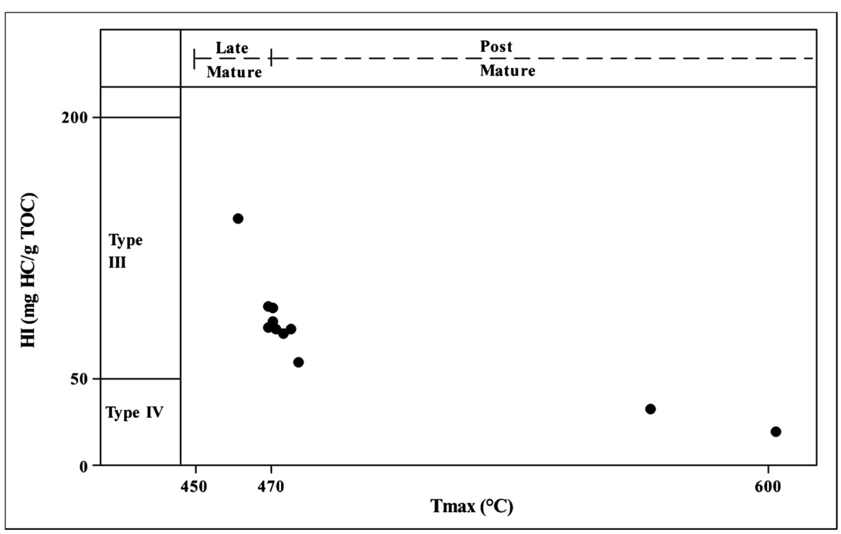

Fig. 4 HI vs T_{max} plot for the Barakar Formation shales from the Jharia Basin

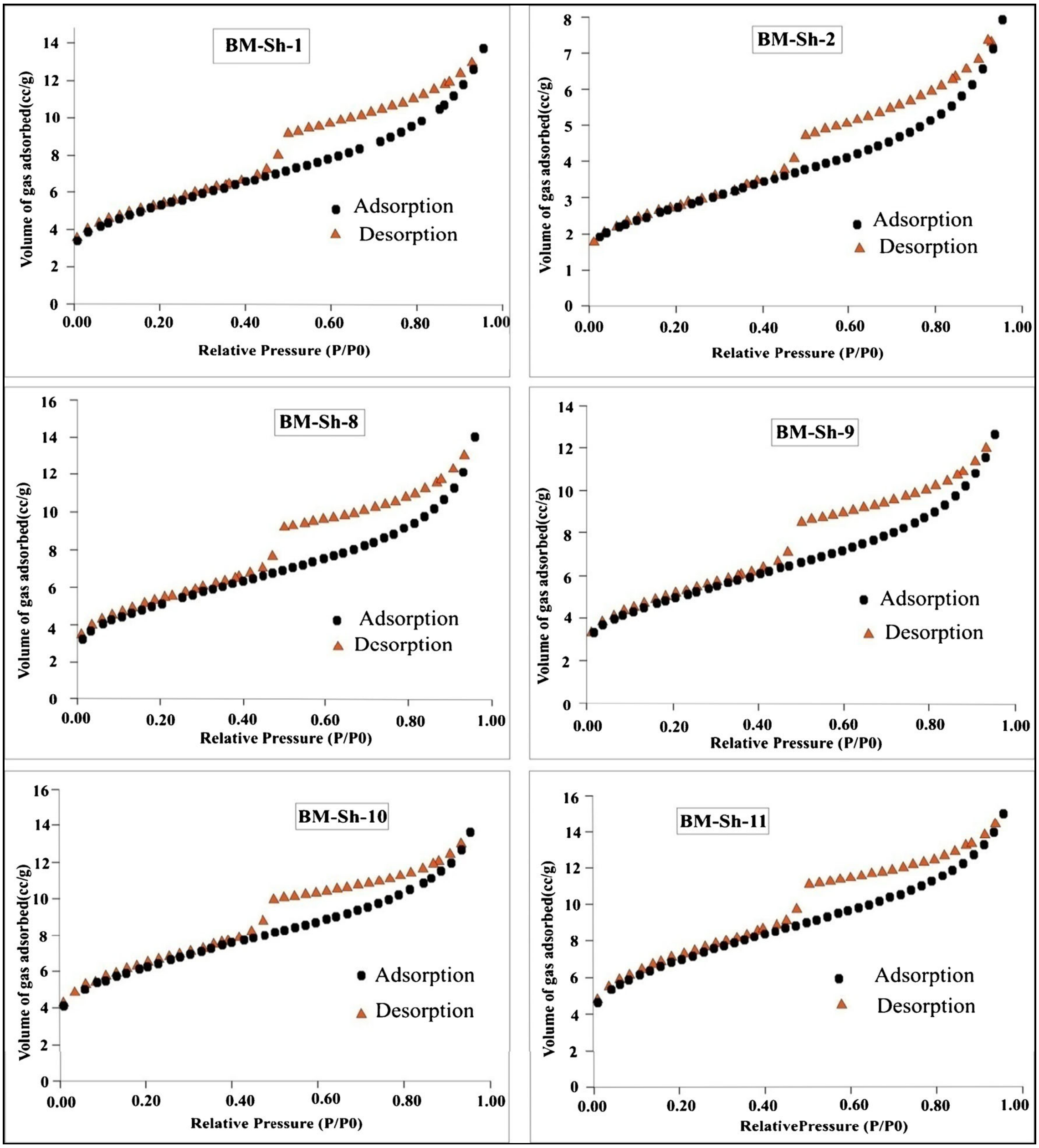

Fig. 5 N_2 adsorption-desorption isotherms of the Barren Measures Formation shales

temperatures were less than the critical temperature of N_2 at 77.35 degrees Kelvin (°K). Sample gas pressure/N_2 saturation pressure ratio (P/P0) measurements enable P0 to be determined automatically at the known sample temperatures of 77.35 K. Pore surface areas, volumes, and pore sizes of each sample were calculated from the recorded data. The Brunauer-Emmett-Teller (BET) specific surface area (BET SSA) was derived over the relative-pressure range of 0.05 to 0.35 (Brunauer et al. 1938).

The commonly used Frenkel-Halsey-Hill (FHH) adsorption isotherm model was utilized to establish the fractal dimensions of the shale samples tested. It involves evaluating equation (i) (Qi et al. 2002; Yao et al. 2008):

$$\ln\left(\frac{V}{V0}\right) = A\left[\ln\left(\ln\left(\frac{P0}{P}\right)\right)\right] + \text{constant} \quad \text{(i)}$$

where

P and P_0 are equilibrium and saturation pressures of the used-gas, respectively;

V and V_0 represent volume of adsorbed gas molecules and monolayer capacity, respectively;

A = power-law exponent which is controlled by the fractal dimension (D) and the means of adsorption.

D is worked out from the slope (S) of the straight-line in the lnV vs ln [ln(P_0/P)] FHH plot using either equation (ii) or (iii).

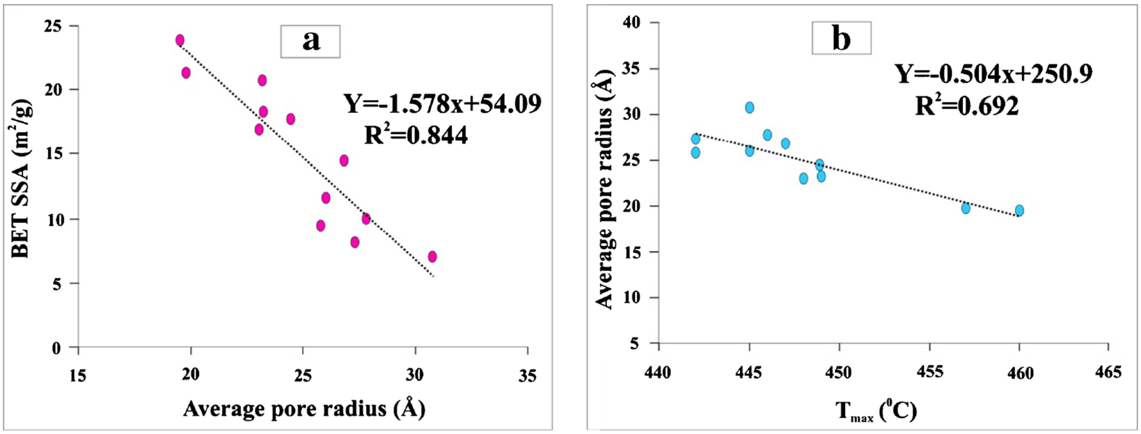

Fig. 7 Barren Measures Formation shale samples: **a** BET SSA versus average pore radius; **b** average pore radius versus T_{max}

$$S = D{-}3 \quad \text{(ii)}$$

$$3S = (D{-}3) \quad \text{(iii)}$$

Together, equations (ii) and (iii) are used in practice to obtain the fractal dimension D (Qi et al. 2002). However, when equation (iii) was used to measure the fractal-metrics, D1 was observed to be negative in all cases, while D2 was observed to be negative in one instance (see Table 4). As fractal values should vary between 2 and 3, the fractal-metrics were calculated only using equation ii.

Results and discussions

Source rock characterization

Barren Measures Formation

The TOC contents of the Barren Measures Formation (BMF) shale samples vary between 2.08 and 6.15 wt%, i.e., within the ranges of "very good" to "excellent" source rock richness (Peters and Cassa 1994). The residual carbon (RC) component of the TOC (1.95 to 4.96 wt%) was observed to be much greater than the pyrolyzable carbon (PC) component (0.13 to 1.19 wt%). Not surprisingly, the RC/PC ratio varied from 4.17 to 15 and was the highest in the most thermally mature shale sample (BM-Sh-11) and least in the shale sample (BM-Sh-7) marked by the highest TOC and hydrogen index (HI) contents (Table 2).

The hydrogen indices of these varied in-between 66 and 206 mg HC/g TOC, signifying predominantly type-III kerogen (Peters and Cassa 1994). Temperature-maxima (T_{max}) of S2 ranged between 442 and 460 °C, i.e., between "early mature" to "peak mature" stages of thermal maturity (Peters and Cassa 1994). The samples with the highest measured thermal maturity levels (BM-Sh-10 and BM-Sh-11) also displayed the lowest S2 and HI values. These relationships are consistent with the expected influence of thermal maturity on petroleum generation and expulsion from source rocks.

Fig. 8 Plot displaying the relationship between BET SSA and BJH pore volume of Jharia Basin Barren Measures Formation shales

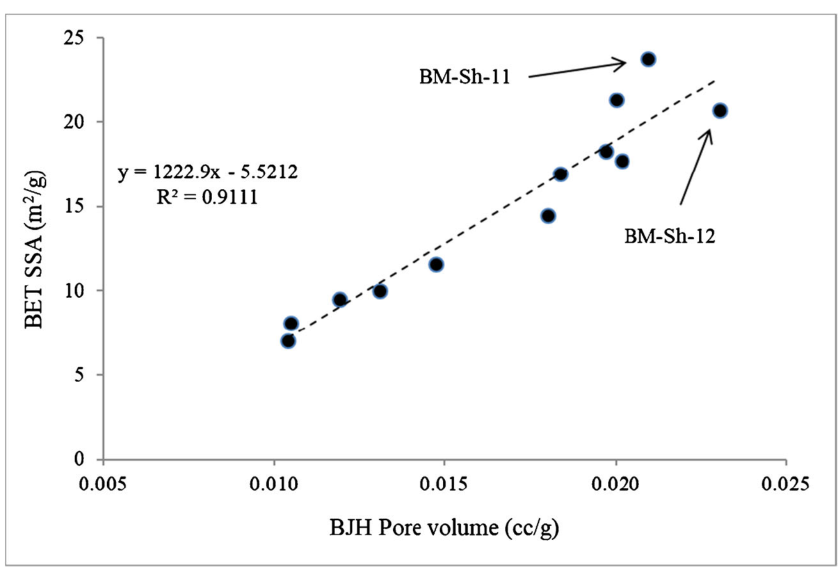

Table 3 Nitrogen gas adsorption results of the collected shale samples

Sample number	BET SSA (m^2/g)	Average pore radius (Å)	BJH pore volume (cc/g)	V_G (cc/g)
BM-Sh-1	18.29	23.24	0.020	13.73
BM-Sh-2	9.49	25.79	0.012	7.91
BM-Sh-3	8.12	27.30	0.011	7.16
BM-Sh-4	14.47	26.81	0.019	12.54
BM-Sh-5	7.04	30.74	0.010	6.99
BM-Sh-6	9.98	27.80	0.013	8.97
BM-Sh-7	11.59	26.01	0.015	9.74
BM-Sh-8	17.72	24.43	0.020	14.00
BM-Sh-9	16.92	23.05	0.018	12.61
BM-Sh-10	21.29	19.78	0.020	13.61
BM-Sh-11	23.77	19.52	0.021	15.00
BM-Sh-12	20.71	23.17	0.023	15.51
Br-Sh-13	3.54	33.28	0.006	3.81
Br-Sh-14	5.77	28.25	0.008	5.27
Br-Sh-15	8.55	20.75	0.008	5.73
Br-Sh-16	10.05	21.06	0.009	6.84
Br-Sh-17	6.16	26.96	0.007	5.36
Br-Sh-18	6.23	27.43	0.008	5.52
Br-Sh-19	4.21	26.43	0.005	3.60
Br-Sh-20	3.54	31.19	0.005	3.57
Br-Sh-21	7.21	24.87	0.008	5.80
Br-Sh-22	4.74	30.38	0.007	4.66
Br-Sh-23	3.57	28.08	0.005	3.24

BET SSA- Brunauer-Emmett-Teller specific surface area; BJH pore volume- Barret-Joyner-Halenda; V_G (cc/g) is the volume of gas adsorbed by the sample

Figure 2 shows the HI-T_{max} cross-plot for the Barren Measures Formation shales. Generally, when shales reach the oil-window stage of maturity, the HI values can be variable depending upon the type of kerogen present. However, once the oil-window is crossed, with some expulsion of petroleum having occurred, the S2 and HI values are reduced. Consequently, the 'peak mature' shales show least HI (Table 2; Fig. 2).

The HI vs TOC cross-plot (Fig. 3) distinguishes the oil and gas generating properties of the Barren Measures and the Barakar Formations. Boundaries displayed in Fig. 3 characterize the nature of the source rock in accordance with the distinctions identified by Jackson et al. (1985). Only sample BM-Sh-7 of the Barren Measures Formation shales falls within the "good oil source" category. This sample is also marked by the lowest RC/PC ratio, i.e., it contains more reactive or pyrolyzable carbon than residual carbon, which is consistent with its better petroleum generation potential than the other samples from Barren

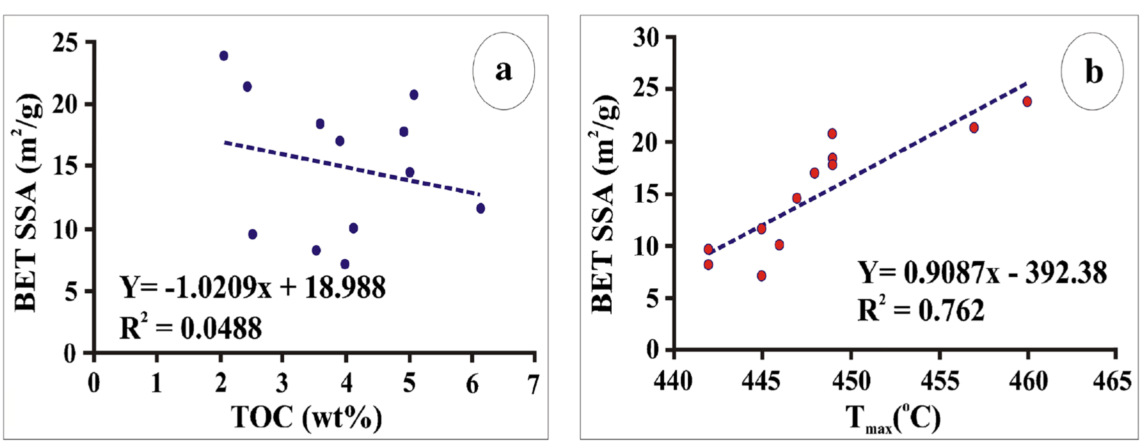

Fig. 6 Barren Measures Formation shale samples: **a** BET SSA versus TOC; **b** BET SSA versus T_{max} (6B)

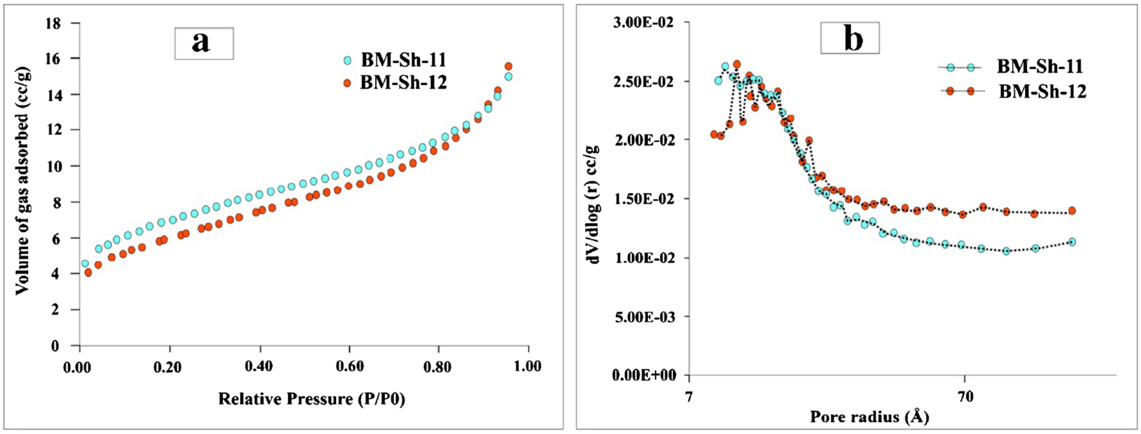

Fig. 9 Adsorption isotherms of samples BM-Sh-11 and BM-Sh-12: **a** at lower relative pressures, the sorption capacity of BM-Sh-11 is higher, while at higher relative pressures, the sorption capacity of BM-Sh-12 exceeds that of BM-Sh-11, owing to its macro-porous character; and **b** dV/dlog(r) vs pore radius for these two samples

Measures Formation. It also displays the maximum S1 value among the Barren Measures Formation shales (Table 2).

Barakar formation

The Barakar Formation shale samples analyzed contain substantially more organic material than the Barren Measures. Their TOC contents vary between 11.20 and 22.78 wt%. The Barakar Formation shale samples are also substantially more thermally mature (T_{max} varies from 461 to 602 °C) than the Barren Measures shales. These samples lie within the condensate/wet-gas and dry-gas windows of thermal maturity (Fig. 4). This is likely to be due to the greater burial depths reached by the Barakar formation than the Barren Measures, allowing them to be exposed to higher temperatures.

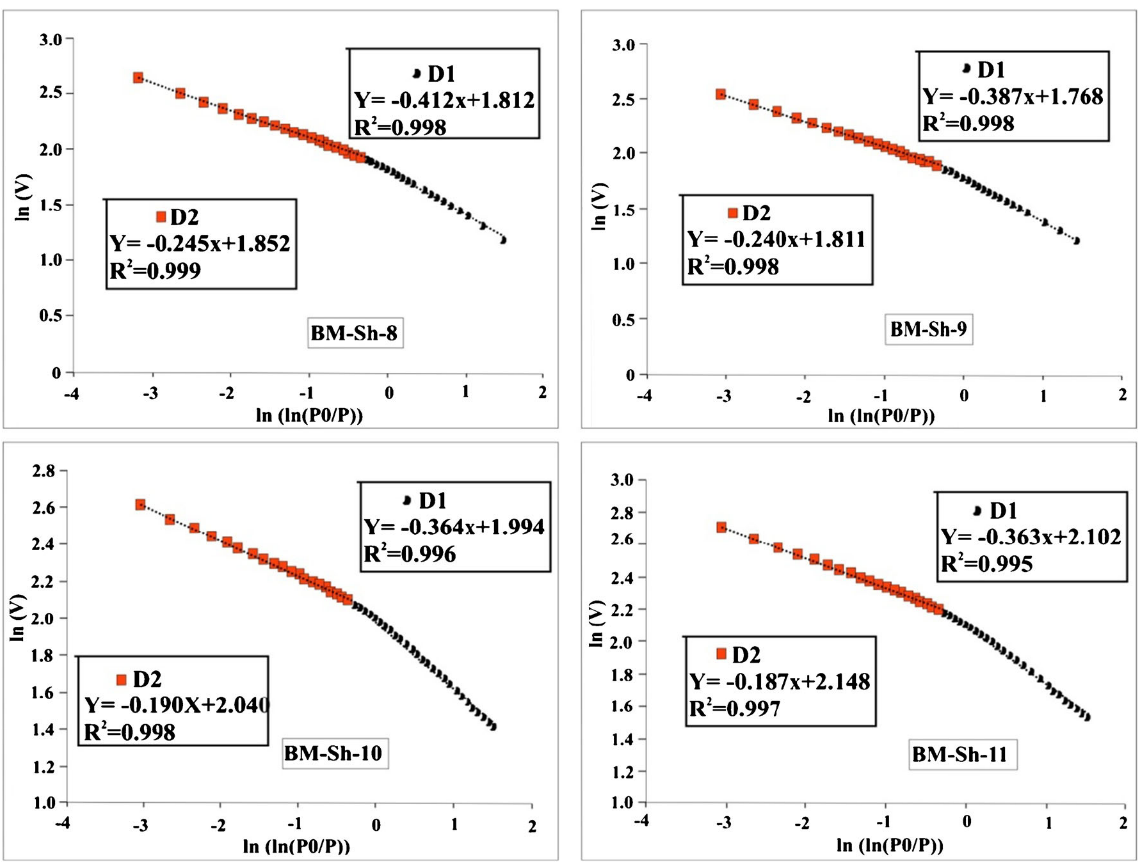

Fig. 10 FHH plot of the Barren Measures shales

Table 4 Fractal parameters calculated using N_2 adsorption data for the Jharia Basin shales

Sample number	P/P0 (0.01–0.50)				P/P0 (0.50–1.00)			
	S_1	R_1^2	D1		S_2	R_2^2	D2	
			3 + S	3 + 3S			3 + S	3 + 3S
BM-Sh-1	−0.397	0.999	2.60	1.81	−0.242	0.997	2.76	2.27
BM-Sh-2	−0.408	0.999	2.59	1.78	−0.272	0.999	2.73	2.18
BM-Sh-3	−0.424	0.999	2.58	1.73	−0.288	0.999	2.71	2.14
BM-Sh-4	−0.448	0.999	2.55	1.66	−0.282	0.996	2.72	2.15
BM-Sh-5	−0.435	0.997	2.57	1.70	−0.322	0.999	2.68	2.03
BM-Sh-6	−0.434	0.999	2.57	1.70	−0.295	0.999	2.71	2.12
BM-Sh-7	−0.394	0.999	2.61	1.82	−0.269	0.999	2.73	2.19
BM-Sh-8	−0.412	0.998	2.59	1.76	−0.245	0.999	2.76	2.27
BM-Sh-9	−0.387	0.998	2.61	1.84	−0.24	0.999	2.76	2.28
BM-Sh-10	−0.384	0.996	2.62	1.85	−0.19	0.998	2.81	2.43
BM-Sh-11	−0.383	0.995	2.62	1.85	−0.187	0.997	2.81	2.44
BM-Sh-12	−0.401	0.998	2.60	1.80	−0.239	0.998	2.76	2.28
Br-Sh-13	−0.457	0.998	2.54	1.63	−0.352	0.999	2.65	1.94
Br-Sh-14	−0.432	0.996	2.57	1.70	−0.3	0.999	2.70	2.10
Br-Sh-15	−0.383	0.986	2.62	1.85	−0.204	0.996	2.80	2.39
Br-Sh-16	−0.382	0.987	2.62	1.85	−0.207	0.999	2.79	2.38
Br-Sh-17	−0.438	0.99	2.56	1.69	−0.293	0.999	2.71	2.12
Br-Sh-18	−0.441	0.994	2.56	1.68	−0.288	0.999	2.71	2.14
Br-Sh-19	−0.367	0.987	2.63	1.90	−0.283	0.999	2.72	2.15
Br-Sh-20	−0.454	0.989	2.55	1.64	−0.33	0.999	2.67	2.01
Br-Sh-21	−0.417	0.988	2.58	1.75	−0.263	0.999	2.74	2.21
Br-Sh-22	−0.464	0.992	2.54	1.61	−0.326	0.999	2.67	2.02
Br-Sh-23	−0.416	0.995	2.58	1.75	−0.297	0.999	2.70	2.11

S_1, R_1^2, and D1 denote the slope of the straight line, coefficient of determination, and fractal dimension, respectively, in the lnV versus ln [ln(P0/P)] FHH plot for the relative pressure range (P/P0) of 0.01–0.50 (Figs. 10 and 14). S_2, R_2^2, and D2 represent the slope of the straight line, coefficient of determination, and fractal dimension respectively, in the lnV versus ln [ln(P0/P)] FHH plot for the relative pressure range (P/P0) of 0.50–1.00 (Figs. 10 and 14).

Previous studies (Pareek 1965; Chakrabarti 1969) have documented that Jharia basin is marked by higher geothermal gradients than the surrounding Permian basins, due to the greater impact of igneous intrusions. The presence of several coal seams at coking ranks within the Barakar Formation is consistent with high heat flows in the basin, which hosts significant reserves of coking coals.

As is the case for the Barren Measures shale samples, the residual carbon (RC) component of TOC (varying from 10.51 to 21.19 wt%) for the Barakar Formation shale samples is much greater than the pyrolyzable carbon (PC) component (varying from 0.43 to 2.13 wt%). The RC/PC ratio was observed to be highest in the thermally mature shales (Table 2). HI varied within the range of 19 to 141 mg HC/g TOC. A strong decreasing trend of HI was observed for these shales with increasing T_{max}. This is consistent with the expectation that with increasing thermal maturity levels, expulsion of hydrocarbons takes place and lowers the present day HI.

The Barakar Formation shale samples show a wider spread on the HI versus TOC cross-plot (Fig. 3). Only the most thermally mature shales (Br-Sh-15 and Br-Sh-16) plot in the "gas source" field. The remaining samples from this formation fall into the "gas and/or oil source" category (Fig. 3) due to their elevated maturity levels. Only the least mature sample, BM-Sh-7, falls within the "good oil source" category on the HI-TOC plot. Furthermore, this shale sample also displays the maximum S1, S2, and HI values among the Barakar Formation shales (Table 2).

N_2 adsorption of barren measures formation shales

Pore structure parameters and pore size distribution

Figure 5 displays the nitrogen-gas adsorption isotherms of the Barren Measures shales. All the samples are marked by considerable hysteresis, indicating the occurrence of capillary

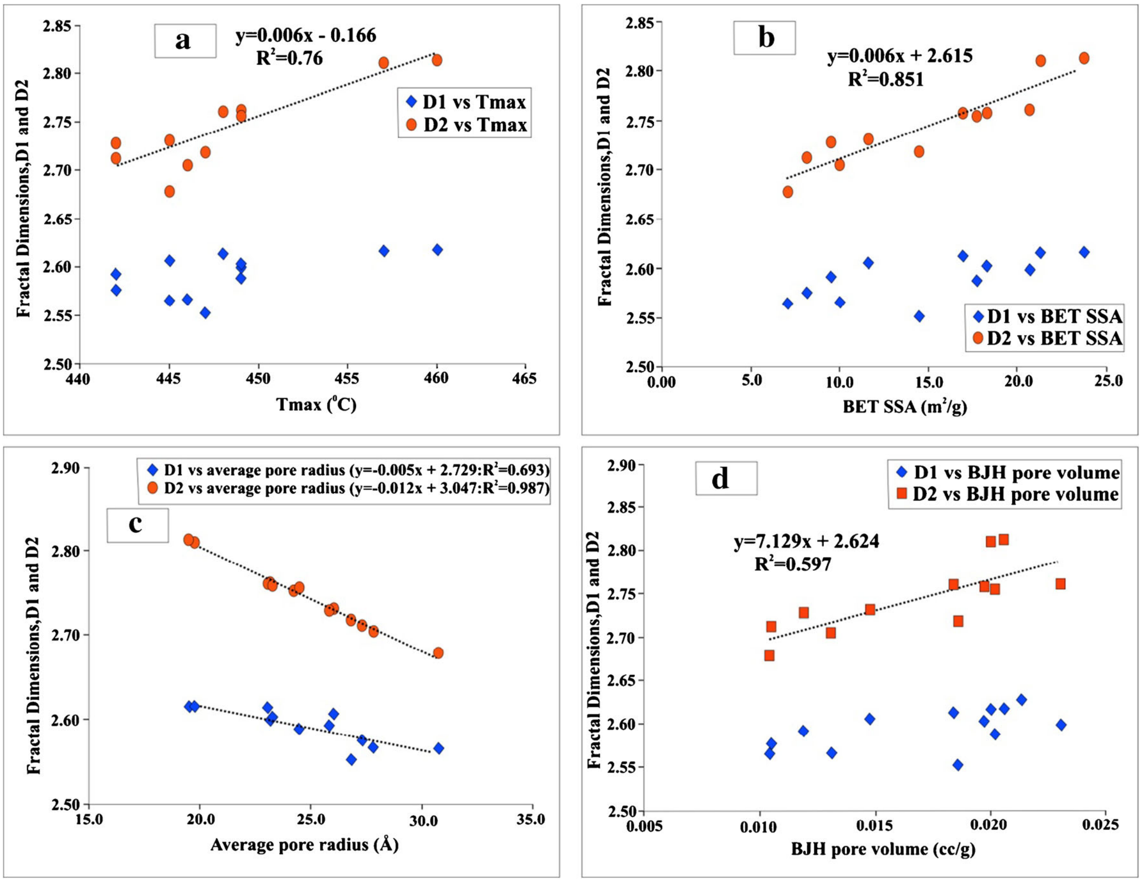

Fig. 11 Cross-plots between fractal dimensions and other pore properties for the Jharia Basin Barren Measures Formation shale samples

condensation within the mesoporous structures (Sing 1985). Hysteresis in adsorption isotherms describes the phenomenon in which desorption isotherms display higher equilibrium moisture contents than absorption at equal temperatures. However, none of the isotherms possess shapes similar to type IV isotherms i.e., absence of any plateau at the end of adsorption isotherms, which are typical of mesoporous materials. None of the isotherm shapes show a "reversible" nature, which is characteristic of type II macroporous materials. Rouquerol et al. (1998) defined these types of isotherms as II-B, which represents a combination of mesoporous and macroporous materials. All the Barren Measures shales displayed H2 hysteresis patterns, which characteristically indicates the presence of "ink-bottle" pore shapes (i.e., narrow neck-wide bodies) (Sing 1985).

The BET SSA of the shales varies within the range of 7.04 and 23.77 m^2/g rock (Table 3). The highest SSA was displayed by sample BM-Sh-11, which also displayed the lowest average pore size, maximum T_{max}, and lowest TOC values. The dependency between SSA of shales and their TOC and/or thermal maturity levels is apparent from studies of several shale basins (Wood and Hazra 2017a). The SSA of

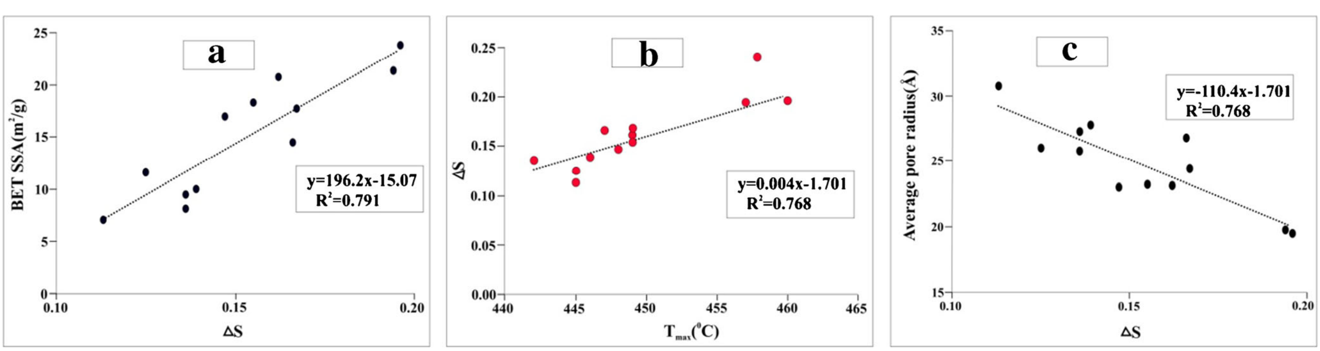

Fig. 12 Cross-plots showing the relationships between the novel fractal-differentiating factor ΔS, and other studied properties for the Jharia Basin Barren Measures Formation shale samples

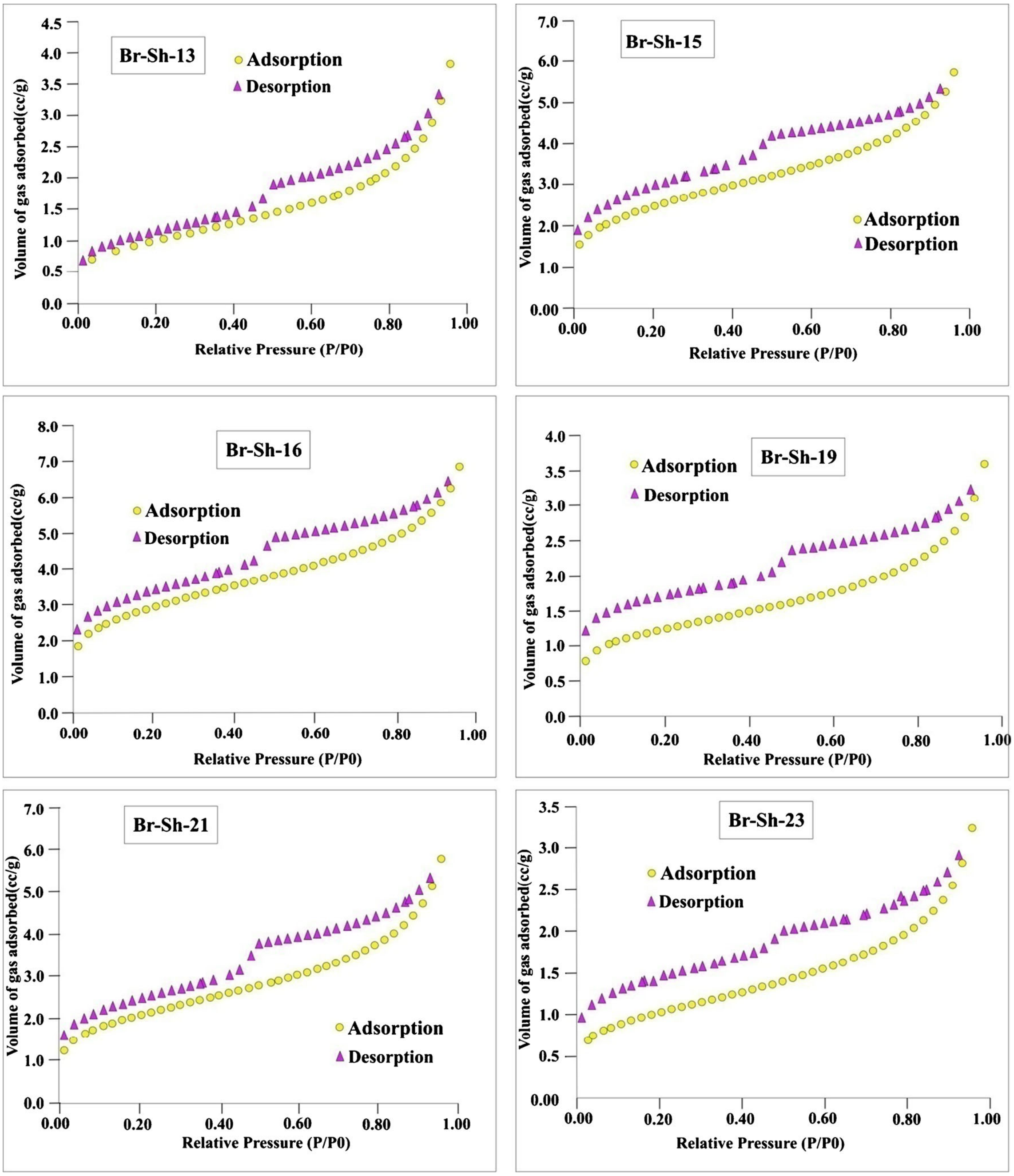

Fig. 13 N_2 gas adsorption-desorption isotherms of the Jharia Basin Barakar Formation shale samples

the Barren Measures shale samples shows no correlation relationship with their TOC contents (Fig. 6a). However, it does display a positive relationship with T_{max} (Fig. 6b). The positive control of maturity levels on SSA in the Jharia Basin Permian shale samples is consistent with earlier findings for Permian shales from other basins of India (Hazra et al. 2018a, b, 2019b).

The SSA shows a negative relationship with average pore sizes of the studied shales (Fig. 7a; $R^2 = 0.84$), which in turn is also influenced by the T_{max} values (Fig. 7b). The most mature shale samples (BM-Sh-10 and BM-Sh-11) display the lowest average pore radii (19.78 and 19.52 Å). These relationships, combined with the lack of any correlation BET SSA with TOC content (Fig. 6a), suggest that thermal maturity is a key controlling factor in the evolution of porous structures within the organic-matter in these shale samples. The average pore radii in these samples varied between 19.52 and 30.74 Å.

The Barret-Joyner-Halenda (BJH) pore volume measurements show a strong positive correlation with the BST SSA values in these shale samples (Fig. 8). Closer examination of Fig. 8, and the data presented in Table 3, reveals that sample BM-Sh-12 has a greater pore volume (0.023 cc/g), than

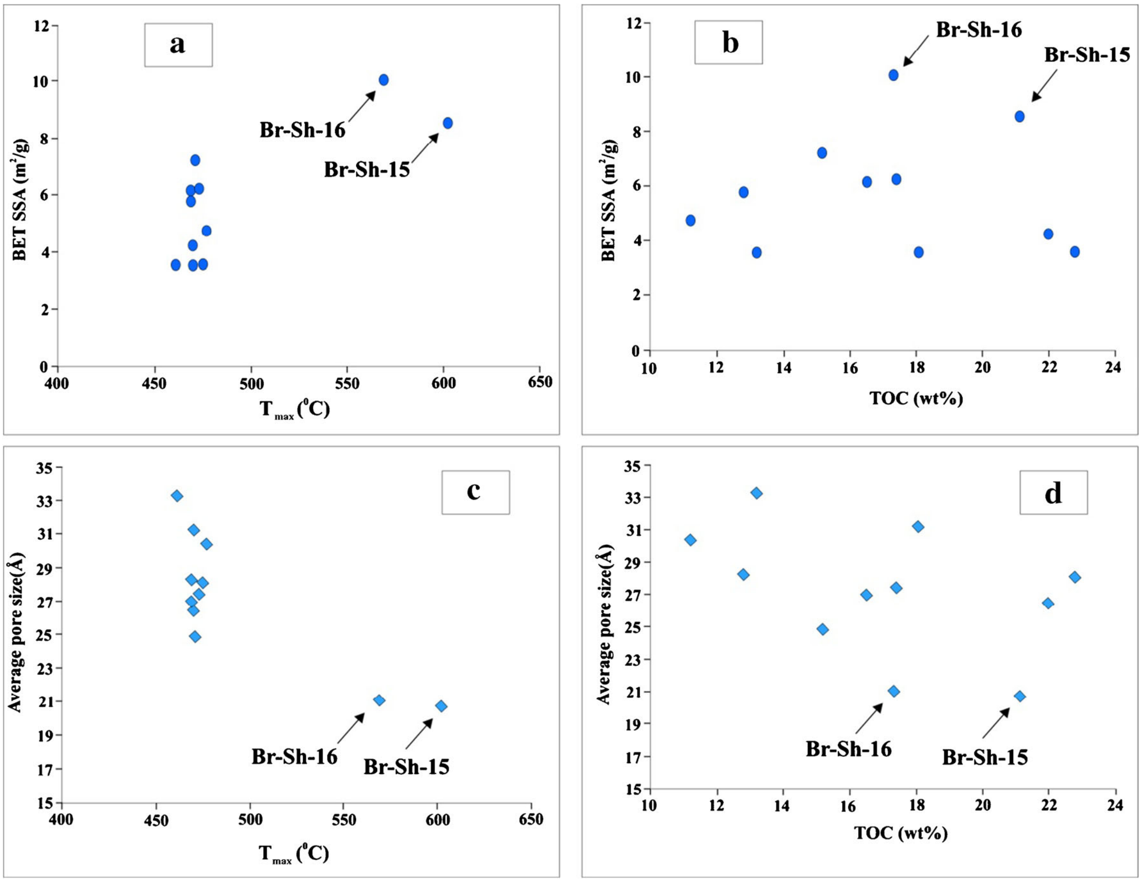

Fig. 14 Jharia Basin Barakar Formation shale samples cross-plot relationships: **a** BET SAA vs thermal maturity; **b** BET SSA vs TOC; **c** average pore size vs thermal maturity; and **d** average pore size vs TOC

sample BM-Sh-11 (0.021), despite having a lower SSA, T_{max}, and larger average pore radius.

Figure 9a plots the adsorption isotherm of samples BM-Sh-11 and BM-Sh-12. These reveal that at up to relative pressure of 0.85, the gas adsorption amount for sample BM-Sh-11 exceeds that of BM-Sh-12. However, beyond that relative pressure, the sorption amount of BM-Sh-12 exceeds the sorption amount of BM-Sh-11; consequently, sample BM-Sh-12 achieves a larger sorption capacity (15.51 cc/g) than sample BM-Sh-11 (15.00 cc/g) from a larger pore volume but smaller SSA, with the volume of adsorbed by its SSA measuring portion being lower. However, at higher relative pressures, owing to the macro-porous character of sample BM-Sh-12, the sorption capacity is increased. The larger average pore radius (Table 3) and the dV/dlog(r) vs pore radius plot (Fig. 9b) also reveal the more macro-porous character of BM-Sh-12 relative to BM-Sh-11.

Fractal dimensions

Figure 10 displays the fractal plots of the Barren Measures Formation shale samples from data listed in Table 4. At lower relative pressures ($P/P0 < 0.50$), the fractal metric D1 varies between 2.55 and 2.62, while higher relative pressure ($P/P0 \geq 0.50 < 1.00$), fractal metric D2 varied between 2.68 and 2.81.

Those Barren Measures Formation shale samples that are the most thermally mature, BM-Sh-10 and BM-Sh-11, display the highest D1 and D2 values (Table 4). In line with pore properties of the Barren Measures shales, the D1 and D2 values display no correlation with TOC contents. On the other hand, D2 displays a positive correlation with T_{max}, whereas D1 values do not display a high correlation with T_{max} (Fig. 11a). Similarly, only a poor correlation exists between BET SSA and D1, while a strong positive correlation is apparent between BET SSA and D2 (Fig. 11b). On the other hand, average pore radius displays a moderate negative correlation with D1 ($R^2 = 0.69$), but a strong negative correlation with D2 ($R^2 = 0.99$; Fig. 11c). The stronger negative relation between D2 and pore size, the positive correlation between D2 and SSA (Fig. 11), and the negative relations between pore sizes and SSA, and with T_{max} (Fig. 7), all indicates that with increase in maturity levels, finer pores are generated, yielding larger surface areas and more complex fractal dimension D2.

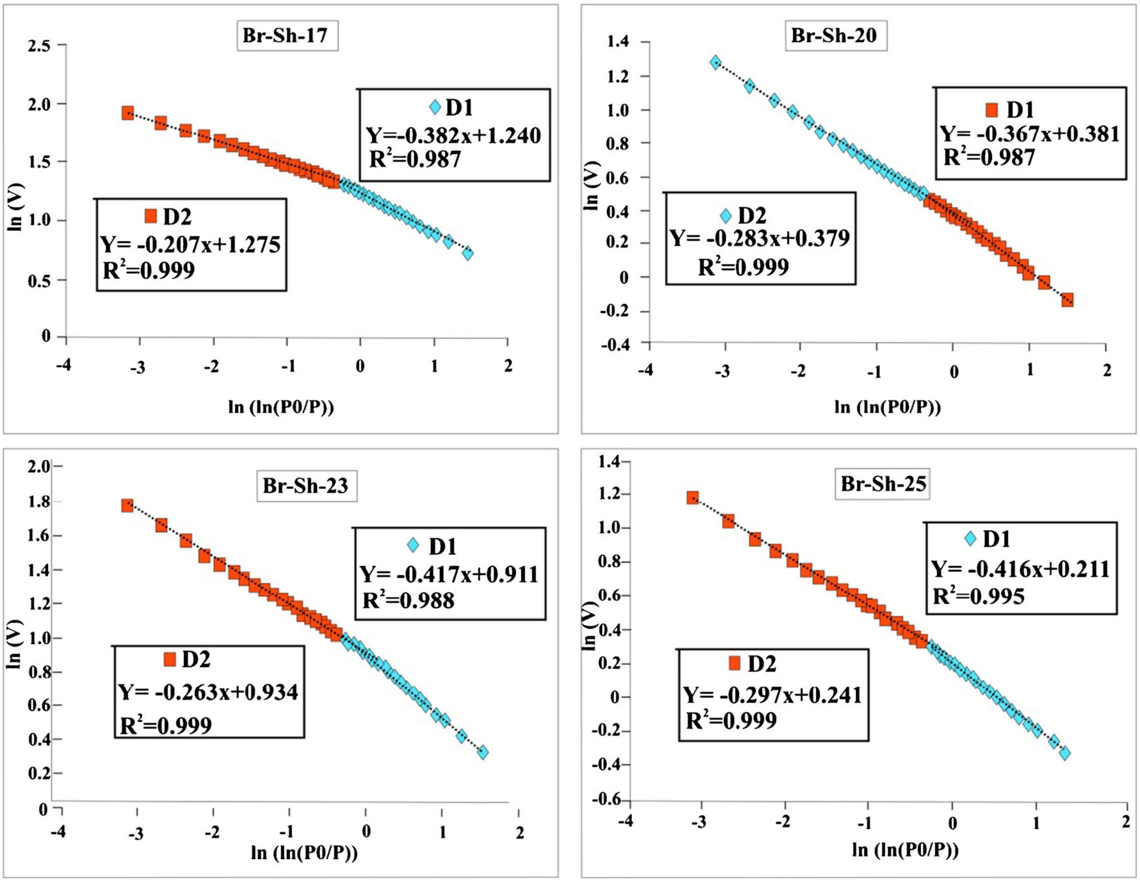

Fig. 15 FHH plot of the Barakar Formation shales

However, the lack of correlation between fractal metric D1 and several pore parameters indicates some complex mechanisms operating in controlling D1, which are not clear from the results presented for the Barren Measures Formation shale samples studied. The inference of macro-porous character for sample BM-Sh-12, as presented in Fig. 9, and already discussed, is also corroborated by its smaller D2 value (i.e., less complex pore structure) relative to samples BM-Sh-10 and BM-Sh-11, although sample BM-Sh-12 has a higher pore volume. As BM-Sh-12 is marked by larger macro-porous structures, its pore volume and radius are higher, while its D2 value is smaller.

The novel fractal-differentiating factor, Δ*S*, recently introduced by Hazra et al. (2018a, b), showed some important relationships. Δ*S* represents the difference between the slopes of the linear portions at P/P0 of 0.5–1.0 and 0–0.5 in the fractal plots, and is expressed by the equation (iv):

$$\Delta S = S^{P/P0:0.5-1.0} - S^{P/P0:0-0.5} \quad \text{(iv)}$$

Δ*S* displays a positive relationship with SSA and T_{max} (Fig. 12a, b), while showing negative relationship with pore sizes (Fig. 12c). These correlations indicate the effect of maturity on pore properties of these shale samples. It further establishes that Δ*S* can be used as a proxy to predict pore structural complexities and peculiarities.

N_2 gas adsorption of the Barakar Formation shales

Figure 13 displays the N_2 gas-adsorption isotherms of the Barakar Formation shales. Similar to the Barren Measures shales, the Barakar Formation shale samples are also marked by considerable hysteresis. They match most closely with the type II-B shape i.e., a combination of meso-porous and macroporous structures (Rouquerol et al. 1998). While for the Barren Measures shale samples total closure of hysteresis loops is apparent, for the Barakar Formation shales for several samples, the hysteresis loops are open. Earlier studies have suggested that the opening of the hysteresis loops is caused by swelling and/or adsorption in the microporous structures of the material (Mastalerz et al. 2012).

By some magnitude, the BET SSA of the Barakar Formation shale samples is substantially smaller (3.54–10.05 m^2/g) than that of the Barren Measures shale samples. This is despite the Barakar Formation shale samples displaying much larger TOC contents and higher thermal maturity levels. The higher thermal maturity levels of these shales, associated with their greater abundance of organic-matter, suggest that they should possess more abundant microporous structures (Pommer and Milliken 2015). However, their low BET SSA values do not support this.

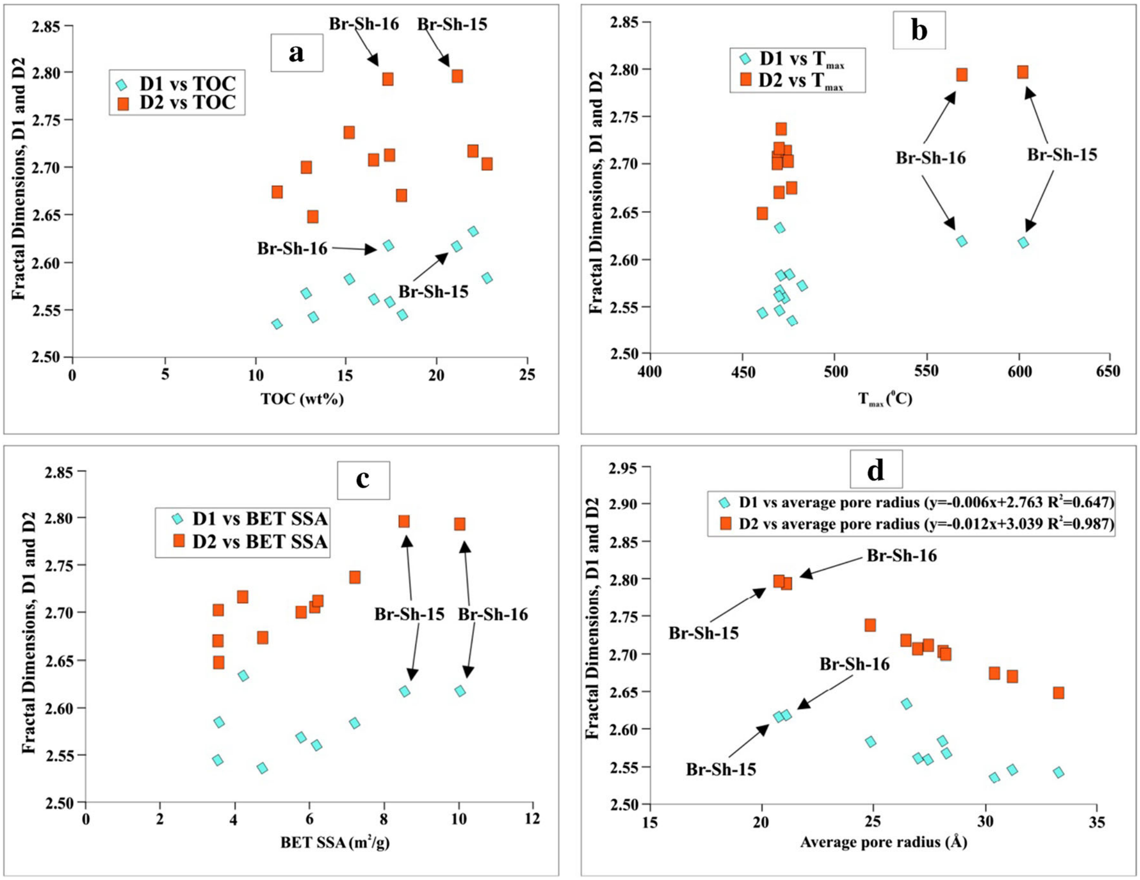

Fig. 16 Cross-plots between fractal dimensions and other pore properties for the Jharia Basin and the Barakar Formation shale samples

Poor correlations exist between SSA of Barakar Formation shales and $T_{\max}$ (Fig. 14a) and TOC (Fig. 14b), especially if samples Br-Sh-15 and Br-Sh-16 are disregarded. Furthermore, only poor correlations exist between the average pore radii and TOC and $T_{\max}$ for the Barakar Formation shale samples (Fig. 14c, d). However, the thermally most mature shales (Br-Sh-15 and Br-Sh-16) display the lowest average pore radii. The lack of any strong relationships for the Barakar Formation shale samples is noteworthy and indicates some peculiarities in the pore properties of these shales. The pore volumes of the Jharia Basin Barakar Formation shale samples are also smaller than that of the Barren Measures shales.

Table 4 shows the details of the fractal parameters calculated for all shale samples. Fractal metrics D1 and D2 vary for the Jharia Basin Barakar Formation shale samples between 2.54 and 2.63 and 2.65 and 2.80, respectively. Although the Barakar Formation shale samples are more mature than the Barren Measures shales, the fractal dimensions for the Barakar Formation shale samples are quite similar and/or smaller than the Jharia Basin Barren Measures Formation shale samples (Fig. 15). The fractal dimensions display relatively poor correlations with TOC, $T_{\max}$, and BET SSA, especially if samples Br-Sh-15 and Br-Sh-16 are disregarded. On the other hand, they display moderate correlations with average pore radius (Fig. 16). These relationships and the existence of only poor correlations displayed in Fig. 14 are indeed conspicuous. They suggest that some peculiarities in the pore properties of the Barakar Formation shale samples also exist.

Discussions

The results presented in this study shows that the Barakar Formation shales, inspite of being thermally more mature and organic-rich, are marked by lower N_2 surface areas, porosities, and fractal dimensions. Generally, with increasing thermal maturity levels, with formation of secondary organic-porosity, surface areas and fractal dimensions increase. At the smallest sizes of micropores, the walls of the pores are very closely spaced. This means that the gas adsorbate and the shale matrix adsorbent need little interaction energy for adsorption to occur. These ultra-small micropores therefore tend to adsorb gas at very low relative pressures (P/P0) (Rouquerol et al. 1998). However, N_2 gas in low pressure adsorption tests is at a very low temperature and probably does not

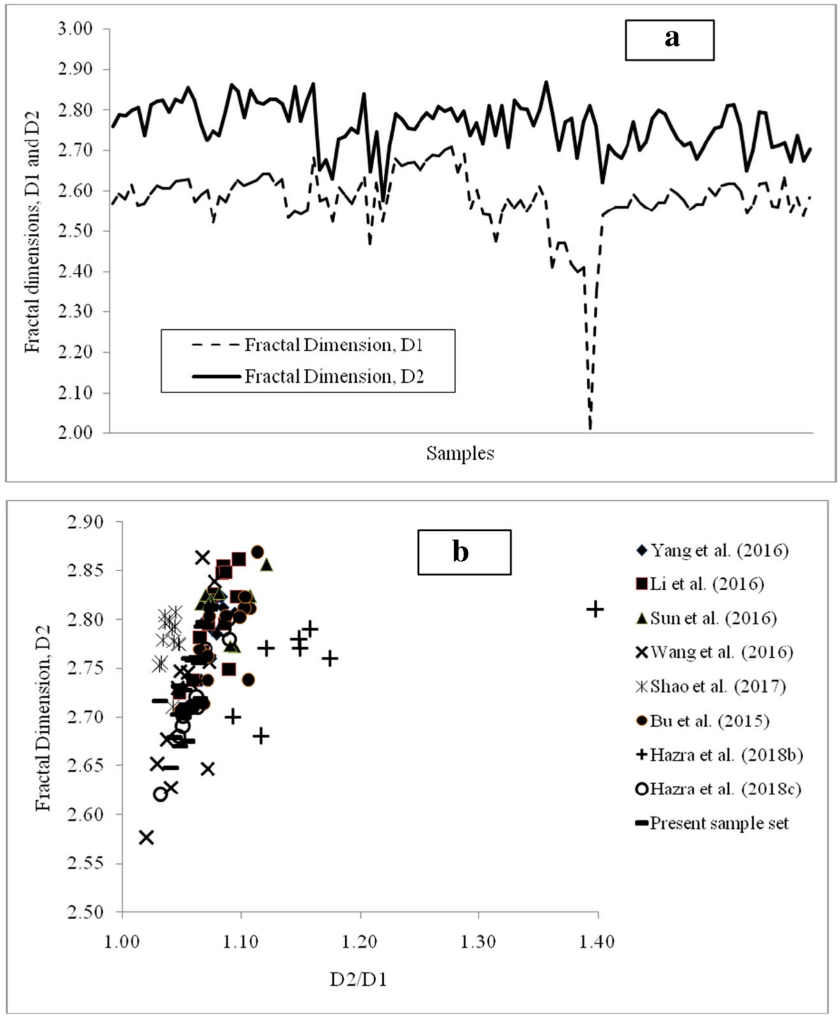

Fig. 17 D1 and D2 values for diverse shale samples, calculated using Eq. ii (the "Nitrogen (N2) gas adsorption "section). The line graph as shown in **a** reveals that D2 is larger than D1 in all the samples considered. Fig. b plots the ratio of D2/D1 vs D2 and also clearly shows that D2 is consistently greater than D1 in all the samples considered. The data includes samples used in this study, and those from Shihezi Formation, Huainan Coalfield, China (Bu et al. 2015); Lower Cambrian Qiongzhusi formation, South China (Li et al. 2016); upper Ordovician Wufeng and lower Silurian Longmaxi Formation shales, Sichuan basin China (Yang et al. 2016a, b); Lower Cambrian and Lower Silurian shale units, upper Yangtze area, China (Wang et al. 2016); Lower Cambrian Niutitang Formation Shale, China (Sun et al. 2016); lower Silurian Longmaxi shales, China (Shao et al. 2017); lower Permian shales, Raniganj basin, India (Hazra et al. 2018a, b)

possess enough thermal energy to gain access to the smaller constricted micropore sizes at low relative pressures. The actual pore structural properties for highly mature or over mature Barakar Formation shales with abundant small-radii microporosity might not be thoroughly accessed using N_2 as the adsorbate.

Furthermore, this lack of ability of N_2 to penetrate and detect complex microporous structures also indicates that the low pressure fractal dimension (D1) might also be undercounted. Figure 17 displays a comparative-plot of D1 and D2 values for 112 diverse published shale samples from several studies focusing on shales from China and India, including those used in this study. For these samples, the fractal D2 values are always larger than D1 values. Lower D1 fractal-dimension values are observed for the 112 shales compared, including some over-mature shale samples with well-developed small-scale micropores. This supports the interpretation that there is a limited access to the finer scale microporosity present in many organic-rich shales during low pressure N_2 gas adsorption tests.

Conclusions

- The Barren Measures Formation shales from the Jharia basin are characterized at "early to peak" thermal maturity and as "very good" to "excellent" source rocks in terms of their TOC contents. All samples analyzed are "fair to good" in terms of their oil-generation potential. The Barakar Formation shale samples are more organic-rich and thermally mature than the Barren Measures Formation shale samples, placing them within the condensate wet-gas and dry-gas windows of thermal maturity.
- N_2 gas adsorption-desorption experiments reveal the Barren Measures shale samples to have high BET SSA, with complex fractal dimensions. Most of the pore properties of these samples are strongly influenced by the thermal maturity levels. On the other hand, quiet conspicuously the Barakar Formation shale samples display lower BET SSA with less-complex fractal dimensions, despite having higher thermal maturities than the Barren Measures shale samples.

- The observed discrepancy related to N_2 gas adsorption data inferred porous structures in relation to organic-richness and thermal maturity levels could possibly be due to the lack of ability of N_2 to penetrate and detect complex microporous structures, resulting in undercounting and improper representation of microporous structures.
- The fractal D1 metric values compared with fractal D2 metric values reported for many shale types across different geological settings and countries is also consistent with the probable inability of low pressure N_2–gas adsorption tests to adequately represent complex microporous structures and the corresponding low-pressure fractal metrics.

Acknowledgments The Director, CSIR-Central Institute of Mining and Fuel Research is acknowledged for giving B. Hazra CSIR-CIMFR inhouse research grant (Project No.: MLP-93/2019-20), the funds of which were utilized to conduct the experiments. The Director, CSIR- Central Institute of Mining and Fuel Research is also acknowledged for giving the necessary infrastructure to conduct low-pressure gas adsorption experiments. The Director, CSIR-National Geophysical Research Institute and Dr. Devleena Mani are thankfully acknowledged for giving necessary permission and conducting the Rock-Eval analysis. The Natural Resources Division, Jamshedpur, Tata Steel Limited is thankfully acknowledged for giving permission and access to borehole cores from the Jharia basin, India.

References

Behar F, Beaumont V, De B, Penteado HL (2001) Rock-Eval 6 technology: performances and developments. Oil Gas Sci Technol Rev Inst Fr Pet Energ Nouv 56:111–134

Boruah A, Ganapathi S (2015) Organic richness and gas generation potential of Permian Barren Measures from Raniganj field, West Bengal, India. J Earth Syst Sci 124(5):1063–1074

Brunauer S, Emmett PH, Teller E (1938) Adsorption of gases in multi molecular layers. J Am Chem Soc 60:309–319

Bu H, Ju Y, Tan J, Wang G, Li X (2015) Fractal characteristics of pores in nonmarine shales from the huainan coalfield, eastern China. J Nat Gas Sci Eng 24:166–177

Carvajal-Ortiz H, Gentzis T (2015) Critical considerations when assessing hydrocarbon plays using Rock-Eval pyrolysis and organic petrology data: data quality revisited. Int J Coal Geol 152:113–122

Chakrabarti AK (1969) On the effects of igneous intrusion on a few coal seams of the Jharia coal field, Bihar, India. Econ Geol 64:319–324

Chatterjee GC, Ghosh PK (1970) Tectonic framework of the peninsular Gondwana of India. Geol Surv India Record 98(2):1–15

CIL (1993) Coal atlas of India. Coal India Limited Calcutta pp. 84–85

Geological Survey of India (1977) Coal resources of India. Mere Geol Surv India 88:575

Godec M, Koperna G, Petrusak R, Oudinot A (2013) Assessment of factors influencing CO2 storage capacity and injectivity in eastern U.S. gas shales. GHGT-11. Energy Procedia 37:6644–6655

EIA (2013) Technically recoverable shale oil and shale gas resources: an assessment of 137 shale formations in 41countries outside the United States. United States Energy Information Administration, US Department of Energy, Washington DC20585 p. XXIV-1 – 42

Fox CS (1930) The Jharia coalfield. Mem Geol Surv India 56

Hazra B, Varma AK, Bandopadhyay AK, Mendhe VA, Singh BD, Saxena VK, Samad SK, Mishra DK (2015) Petrographic insights of organic matter conversion of Raniganj basin shales, India. Int J Coal Geol 150-151:193–209

Hazra B, Dutta S, Kumar S (2017) TOC calculation of organic matter rich sediments using Rock-Eval pyrolysis: critical consideration and insights. Int J Coal Geol 169:106–115

Hazra B, Wood DA, Vishal V, Varma AK, Sakha D, Singh AK (2018a) Porosity controls and fractal disposition of organic-rich Permian shales using low- pressure adsorption techniques. Fuel 220:837–848

Hazra B, Wood DA, Kumar S, Saha S, Dutta S, Kumari P, Singh AK (2018b) Fractal disposition and porosity characterization of lower Permian Raniganj Basin Shales, India. J Nat Gas Sci Eng 59:452–465

Hazra B, Wood DA, Mani D, Singh PK, Singh AK (2019a) Source-rock geochemistry: organic content, type, and maturity. In: Evaluation of Shale Source Rocks and Reservoirs. Petroleum Engineering. Springer, Cham

Hazra B, Wood DA, Mani D, Singh PK, Singh AK (2019b) Organic and inorganic porosity, and controls of hydrocarbon storage in Shales. In: Evaluation of Shale Source Rocks and Reservoirs. Petroleum Engineering. Springer, Cham

Hazra B, Wood DA, Mani D, Singh PK, Singh AK (2019c) Source-rock evaluation using the Rock-Eval technique. In: Evaluation of Shale Source Rocks and Reservoirs. Petroleum Engineering. Springer, Cham

Hazra B, Karacan CÖ, Mani D, Singh PK, Singh AK (2019d) Insights from Rock-Eval analysis on the influence of sample weight on hydrocarbon generation from lower Permian organic matter rich rocks, west Bokaro basin, India. Mar Pet Geol 106:160–170

Holmes R, Rupp E, Vishal V, Wilcox J (2017) Selection of shale preparation protocol and outgas procedures for applications in low-pressure analysis. Energy Fuel 31(9):9043–9051

Jackson KS, Hawkins PJ, Bennett AJR (1985) Regional facies and geochemical, evaluation of southern Denison trough. APEA J 20:143–158

Jarvie DM (2012a) Shale resource systems for oil and gas: part 1—shale–gas resource systems. In: Breyer JA (ed) Shale Reservoirs—Giant Resources for the 21st Century. AAPG Mem, vol 97, pp 69–87

Jarvie DM (2012b) Shale resource systems for oil and gas: part 2—shale–oil resource systems. In: Breyer JA (ed) Shale Reservoirs—Giant Resources for the 21st Century. AAPG Mem, vol 97, pp 89–119

Jarvie DM, Hill RJ, Ruble TE, Pollastro RM (2007) Unconventional shale gas systems: the Mississippian Barnett Shale of north-central Texas as one model for thermogenic shale-gas assessment. AAPG Bull 91(4):475–500

Lafargue E, Espitalié J, Marquis F, Pillot D (1998) Rock–Eval 6 applications in hydrocarbon exploration, production, and soil contamination studies. Inst Fr Pét 53:421–437

Li A, Ding W, He J, Dai P, Yin S, Xie F (2016) Investigation of pore structure and fractal characteristics of organic-rich shale reservoir: a case study of Lower Cambrian Qiongzhusi formation in Malong block of eastern Yunnan Province, South China. Mar Pet Geol 70: 46–57

Loucks RG, Reed RM, Ruppel SC, Jarvie DM (2009) Morphology, genesis, and distribution of nanometer-scale pores in siliceous mudstones of the Mississippian Barnett Shale. J Sediment Res 79:848–861

Loucks RG, Reed RM, Ruppel SC, Hammes U (2012) Spectrum of pore types and networks in mudrocks and a descriptive classification for matrix-related mudrock pores. AAPG Bull 96:1071–1098

Mastalerz M, He L, Melnichenko YB, Rupp JA (2012) Porosity of coal and shale: insights from gas adsorption and SANS/USANS techniques. Energy Fuel 26(8):5109–5120

Mastalerz M, Schimmelmann A, Drobniak A, Chen Y (2013) Porosity of Devonian and Mississippian New Albany Shale across a maturation

gradient: insights from organic petrology, gas adsorption, and mercury intrusion. AAPG Bull 97:1621–1643
Mendhe VA, Mishra S, Varma AK, Kamble AD, Bannerjee M, Sutay T (2017) Gas reservoir characteristics of the Lower Gondwana Shales in Raniganj Basin of Eastern India. J Pet Sci Eng 149:649–664
Merey S, Sinayuc C (2016) Analysis of carbon dioxide sequestration in shale gas reservoirs by using experimental adsorption data and adsorption models. J Nat Gas Sci Eng 36:1087–1105
Mishra HK, Cook AC (1992) Petrology and thermal maturity of coals in the Jharia Basin. Implications for Oil and Gas Origins. Int J Coal Geol 20:277–313
Mishra HK, Chandra TK, Verma RP (1990) Petrology of some Permian coals of India. Int J Coal Geol 16:47–71
Mukhopadhyay G, Mukhopadhyay SK, Roychowdhury M, Parui PK (2010) Stratigraphic correlation between different Gondwana basins of India. J Geol Soc India 76:251–266
Pareek HS (1965) Petrological characteristics of Barakar coal seams, metamorphosed by lamprophyre sill in the jharia coalfield, Bihar. Proc Indian Acad Sci - Sect B 63(5):261–270
Peters J (2000) Evaluation of coalbed methane potential of Jharia Basin, India. *SPE* 64457 presented at Asia Pacific Oil and Gas Conference and Exhibition held in Brisbane, Australia, 16–18 October
Peters KE, Cassa, M.R (1994) Applied source rock geochemistry. In: Magoon LB, Dow WG (Eds.) The Petroleum System d from Source to Trap. AAPG Mem 60:93–120
Peters KE, Xia X, Pomerantz AE, Mullins OC (2016) Geochemistry applied to evaluation of unconventional resources. In: Ma YZ, Holditch SA (eds) Unconventional oil and gas resources handbook: evaluation and development. Gulf Professional Publishing, Waltham, pp 71–126
Pommer M, Milliken K (2015) Pore types and pore-size distributions across thermal maturity, eagle ford formation, southern Texas. AAPG Bull 99:1713–1744
Press Information Bureau, Government of India, Ministry of Petroleum & Natural Gas, 31-July-2015. https://pib.gov.in/newsite/PrintRelease.aspx?relid=124078
Psarras P, Holmes R, Vishal V, Wilcox J (2017) Methane and CO2 adsorption capacities of kerogen in the Eagle Ford shale from molecular simulation. Acc Chem Res 50(8):1818–1828
Qi H, Ma J, Wong P (2002) Adsorption isotherms of fractal surfaces. Colloids Surf A Physicochem Eng Asp 206:401–407
Ross DJK, Bustin RM (2009) The importance of shale composition and pore structure upon gas storage potential of shale gas reservoirs. Mar Pet Geol 26:916–927
Rouquerol J, Rouquerol F, Sing KSW (1998) Absorption by powders and porous solids. Academic press ISBN 0080526012
Schmoker JW (1995) Method for assessing continuous-type (unconventional) hydrocarbon accumulations, in D L Gautier, G L Dolton, K I Takahashi, and K L Varnes, eds., 1995 National assessment of United States oil and gas resources– Results, methodology, and supporting data: US Geological Survey Digital Data Series 30, CD-ROM
Shao X, Pang X, Li Q, Wang P, Chen D, Shen W, Zhao Z (2017) Pore structure and fractal characteristics of organic-rich shales: a case study of the lower Silurian Longmaxi shales in the Sichuan Basin, SW China. Mar Pet Geol 80:192–202
Sing KS (1985) Reporting physisorption data for gas/solid systems with special reference to the determination of surface area and porosity (recommendations 1984). Pure Appl Chem 57(4):603–619
Singh AK, Singh MP, Sharma M, Srivastava SK (2007) Microstructures and microtextures of natural cokes: a case study of heat-altered coking coals from the Jharia Coalfield, India. Int J Coal Geol 71: 153–175
Singh AK, Singh MP, Sharma M (2008) Genesis of natural cokes: some Indian examples. Int J Coal Geol 75:40–48
Singh AK, Sharma M, Singh MP (2013) SEM and reflected light petrography: a case study on natural cokes from seam XIV, Jharia coalfield, India. Fuel 112:502–512
Sun M, Yu B, Hu Q, Chen S, Xia W, Ye R (2016) Nanoscale pore characteristics of the lower Cambrian Niutitang formation shale: a case study from well Yuke #1 in the Southeast of Chongqing, China. Int J Coal Geol 154-155:16–29
Tissot BP, Welte DH (1978) Petroleum formation and occurrence: a new approach to oil and gas exploration. Springer-Verlag, Berlin
Vaid M (2017) India's shale gas prospects. Oil Gas Finan J 14(5):42–43
Varma AK, Hazra B, Samad SK, Panda S, Mendhe VA (2014) Methane sorption dynamics and hydrocarbon generation of shale samples from West Bokaro and Raniganj basins, India. J Nat Gas Sci Eng 21:1138–1147
Varma AK, Hazra B, Chinara I, Mendhe VA, Dayal AM (2015) Assessment of organic richness and hydrocarbon generation potential of Raniganj basin shales, West Bengal, India. Mar Pet Geol 59: 480–490
Vishal V, Ranjith PG, Pradhan SP, Singh TN (2013a) Permeability of sub-critical carbon dioxide in naturally fractured Indian bituminous coal at a range of down-hole stress conditions. Eng Geol 167:148–156
Vishal V, Ranjith PG, Singh TN (2013b) CO_2 permeability of Indian bituminous coals: implications for carbon sequestration. Int J Coal Geol 105:36–47
Vishal V, Chandra D, Bahadur J, Sen D, Hazra B, Mahanta B, Tiwari DM (2019) Interpreting pore dimensions in gas shales using a combination of SEM imaging, small-angle neutron scattering, and low-pressure gas adsorption. Energy Fuel 33(6):4835–4848
Wang Y, Zhu Y, Liu S, Zhang R (2016) Pore characterization and its impact on methane adsorption capacity for organic-rich marine shales. Fuel 181:227–237
Wood DA, Hazra B (2017a) Characterization of organic-rich shales for petroleum exploration & exploitation: a review- part 1: bulk properties, multi-scale geometry and gas adsorption. J Earth Sci 28(5): 739–757
Wood DA, Hazra B (2017b) Characterization of organic-rich shales for petroleum exploration & exploitation: a review- part 2: geochemistry, thermal maturity, isotopes and biomarkers. J Earth Sci 28(5): 758–778
Yang F, Ning Z, Liu H (2014) Fractal characteristics of shales from a shale gas reservoir in the Sichuan Basin, China. Fuel 115:378–384
Yang F, Ning Z, Wang Q, Zhang R, Krooss BM (2016a) Pore structure characteristics of lower Silurian shales in the southern Sichuan Basin, China: insights to pore development and gas storage mechanism. Int J Coal Geol 156:12–24
Yang R, He S, Yi J, Hu Q (2016b) Nano-scale pore structure and fractal dimension of organic-rich Wufeng-Longmaxi shale from Jiaoshiba area, Sichuan Basin: investigations using FE-SEM, gas adsorption and helium pycnometry. Mar Pet Geol 70:27–45
Yao Y, Liu D, Tang D, Tang S, Huang W (2008) Fractal characterization of adsorption-pores of coals from North China: an investigation on CH4 adsorption capacity of coals. Int J Coal Geol 73:27–42
Zhang T, Ellis GE, Ruppel SC, Milliken KL, Yang R (2012) Effect of organic matter type and thermal maturity on methane adsorption in shale-gas systems. Org Geochem 47:120–131